

- [3] J. H. Kim, H. J. Chun, I. P. Hong, Y. J. Kim, and Y. B. Park, "Analysis of FSS radomes based on physical optics method and ray tracing technique," *IEEE Antennas Wireless Propag. Lett.*, vol. 13, pp. 868–871, May 2014.
- [4] S. M. A. M. H. Abadi, M. Li, and N. Behdad, "Harmonic-suppressed miniaturized-element frequency selective surfaces with higher order bandpass responses," *IEEE Trans. Antennas Propag.*, vol. 62, no. 5, pp. 2562–2571, May 2014.
- [5] S. Celozzi, R. Araneo, and G. Lovat, *Electromagnetic Shielding*. Hoboken, NJ, USA: Wiley, 2008.
- [6] I. S. Syed, Y. Ranga, L. Matekovits, K. P. Esselle, and S. G. Hay, "A single-layer frequency-selective surface for ultrawideband electromagnetic shielding," *IEEE Trans. Electromagn. Compat.*, vol. 56, no. 6, pp. 1404–1411, Dec. 2014.
- [7] S. Keyrouz, G. Perotto, and H. J. Visser, "Frequency selective surface for radio frequency energy harvesting applications," *IET Microw. Antennas Propag.*, vol. 8, no. 7, pp. 523–531, May 2014.
- [8] P. Wu, F. Bai, Q. Xue, X. Liu, and S. Y. R. Hui, "Use of frequency-selective surfaces for suppressing radio-frequency interference from wireless charging pads," *IEEE Trans. Ind. Electron.*, vol. 61, no. 8, pp. 3969–3977, Aug. 2014.
- [9] H. Zhou *et al.*, "Ultra-wideband frequency selective surface," *Electron. Lett.*, vol. 48, no. 1, pp. 11–13, Jan. 2012.
- [10] X.-C. Zhu *et al.*, "Design of a bandwidth-enhanced polarization rotating frequency selective surface," *IEEE Trans. Antennas Propag.*, vol. 62, no. 2, pp. 940–944, Feb. 2014.
- [11] Y. Li, L. Li, Y. Zhang, and C. Zhao, "Design and synthesis of multi-layer frequency selective surface based on antenna-filter-antenna using minkowski fractal structures," *IEEE Trans. Antennas Propag.*, vol. 63, no. 1, pp. 133–141, Jan. 2015.
- [12] B. Sanz-Izquierdo and E. A. Parker, "3D printing technique for fabrication of frequency selective structures for built environment," *Electron. Lett.*, vol. 49, no. 18, pp. 1117–1118, Aug. 2013.
- [13] B. Sanz-Izquierdo and E. A. Parker, "3D printing of elements in frequency selective arrays," *IEEE Trans. Antennas Propag.*, vol. 62, no. 12, pp. 6060–6066, Dec. 2014.
- [14] B. Li and Z. Shen, "Three-dimensional dual-polarized frequency selective structure with wide out-of-band rejection," *IEEE Trans. Antennas Propag.*, vol. 62, no. 1, pp. 130–137, Jan. 2014.
- [15] I. G. Lee and I. P. Hong, "3D frequency selective surface for stable angle of incidence," *Electron. Lett.*, vol. 50, no. 6, pp. 423–424, Mar. 2014.
- [16] F. C. Huang, C. N. Chiu, T. L. Wu, and Y. P. Chiou, "Very closely located dual-band frequency selective surfaces via identical resonant elements," *IEEE Antennas Wireless Propag. Lett.*, vol. 14, pp. 414–417, Feb. 2015.
- [17] B. Sanz-Izquierdo and E. A. Parker, "Dual polarized reconfigurable frequency selective surfaces," *IEEE Trans. Antennas Propag.*, vol. 62, no. 2, pp. 764–771, Feb. 2014.
- [18] L. Zhang, G. Yang, Q. Wu, and J. Hua, "A novel active frequency selective surface with wideband tuning range for EMC purpose," *IEEE Trans. Magn.*, vol. 48, no. 11, pp. 4534–4537, Nov. 2012.
- [19] K. Sarabandi and N. Behdad, "A frequency selective surface with miniaturized elements," *IEEE Trans. Antennas Propag.*, vol. 55, no. 5, pp. 1239–1245, May 2007.
- [20] H. L. Liu, K. L. Ford, and R. J. Langley, "Design methodology for miniaturized frequency selective surface using lumped reactive components," *IEEE Trans. Antennas Propag.*, vol. 57, no. 9, pp. 2732–2738, Sep. 2009.
- [21] F. Bayatpur and K. Sarabandi, "Single-layer high-order miniaturized-element frequency-selective surfaces," *IEEE Trans. Antennas Propag.*, vol. 56, no. 4, pp. 774–781, Apr. 2008.
- [22] X. D. Hu, X. L. Zhou, L. S. Wu, L. Zhou, and W. Y. Yin, "A miniaturized dual-band frequency selective surface (FSS) with closed loop and its complementary pattern," *IEEE Antennas Wireless Propag. Lett.*, vol. 8, pp. 1374–1377, Jan. 2009.
- [23] C. N. Chiu and K. P. Chang, "A novel miniaturized-element frequency selective surface having a stable resonance," *IEEE Antennas Wireless Propag. Lett.*, vol. 8, pp. 1175–1177, Nov. 2009.
- [24] G. Yang, T. Zhang, W. Li, and Q. Wu, "A novel stable miniaturized frequency selective surface," *IEEE Antennas Wireless Propag. Lett.*, vol. 9, pp. 1018–1021, Nov. 2010.
- [25] M. Yan *et al.*, "A novel miniaturized frequency selective surface with stable resonance," *IEEE Antennas Wireless Propag. Lett.*, vol. 13, pp. 639–641, Apr. 2014.
- [26] Y. M. Yu, C. N. Chiu, Y. P. Chiou, and T. L. Wu, "A novel 2.5-dimensional ultraminiaturized-element frequency selective surface," *IEEE Trans. Antennas Propag.*, vol. 62, no. 7, pp. 3657–3663, Jul. 2014.
- [27] Y. M. Yu, C. N. Chiu, Y. P. Chiou, and T. L. Wu, "An effective via-based frequency adjustment and minimization methodology for single-layered frequency selective surfaces," *IEEE Trans. Antennas Propag.*, vol. 63, no. 4, pp. 1641–1649, Apr. 2015.
- [28] Y. Shi, W. Tang, W. Zhuang, and C. Wang, "Miniaturized frequency selective surface based on 2.5-dimensional closed loop," *Electron. Lett.*, vol. 50, no. 23, pp. 1656–1658, Nov. 2014.
- [29] C.-D. Wang *et al.*, "Bandwidth enhancement based on optimized via location for multiple vias EBG power/ground planes," *IEEE Trans. Compon. Packag. Manuf. Technol.*, vol. 2, no. 2, pp. 332–341, Feb. 2012.

## All-Metal Antenna Array Based on Microstrip Line Structure

Le Chang, Zhijun Zhang, Yue Li, and Zhenghe Feng

**Abstract**—In this communication, an all-metal standing wave antenna array is proposed based on the microstrip transmission line. By alternatively blocking the microstrip line every half wavelength, the symmetrical equivalent magnetic currents are broken for effectively radiating. By properly tuning the blocking positions along the microstrip line, a broadside pattern is achieved with high gain. The proposed antenna is scalable along one direction to a certain level to acquire the directivity as high as about 15 dBi. More importantly, the proposed antenna array has the potential to be built only by metal without any dielectrics. The all-metal structure has the merits of being low-cost, light weight, easily fabricated, and having no dielectric losses. Based on this idea, a five-segment linear array with a center feed is designed and tested. The measured bandwidth is from 7.83 to 8.81 GHz (980 MHz, 11.78%), and the measured gain is ranging from 9.1 to 12.47 dBi.

**Index Terms**—Antenna array, antenna radiation pattern, microstrip antennas, transmission lines.

### I. INTRODUCTION

Microstrip line is the most popular planar transmission line due to the simple photographic printing process and easy integration with other passive or active microwave devices [1]. Microstrip lines cannot radiate effectively themselves as shown in Fig. 1(a). According to the "LOVE equivalent theorem" [2], the equivalent magnetic currents along one side of the line are reversed with the counterparts along the other side. However, the phases of the magnetic currents reverse every half wavelength, if the magnetic currents of every half wave can be alternatively removed as illustrated in Fig. 1(b), where in-phase magnetic currents are left and effective radiation can be achieved.

Manuscript received July 11, 2015; revised September 26, 2015; accepted November 11, 2015. Date of publication November 17, 2015; date of current version December 31, 2015. This work was supported in part by the National Basic Research Program of China (contract 2013CB329002) and in part by the National High Technology Research and Development Program of China (863 Program; contract 2011AA010202), in part by the National Natural Science Foundation of China (contract 61371012), in part by the National Science and Technology Major Project of the Ministry of Science and Technology of China (2013ZX03003008-002), and in part by a China Postdoctoral Science Foundation funded project (2015T80084).

The authors are with the State Key Lab on Microwave and Communications, Tsinghua National Laboratory for Information Science and Technology, Tsinghua University, Beijing 100084, China (e-mail: zjzh@tsinghua.edu.cn; lye@mails.tsinghua.edu.cn).

Color versions of one or more of the figures in this communication are available online at <http://ieeexplore.ieee.org>.

Digital Object Identifier 10.1109/TAP.2015.2500907

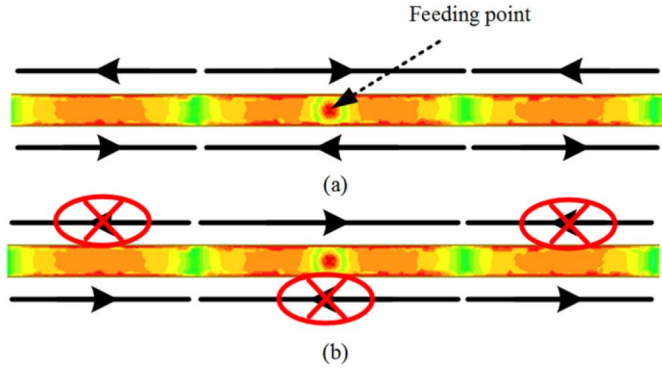


Fig. 1. (a) Equivalent magnetic currents of the microstrip line's fringing fields. (b) Schematic diagram for effective radiation.

Removal of the magnetic currents can be done by shorting them to the ground. Similar method has been used to design a travelling wave antenna in [3]. The reported antenna was a microstrip leaky wave antenna featuring the backward to forward scanning capability. The antenna was fabricated using the printed circuit board processing technology. It consisted of 10 cascaded half-width microstrip patches, and a peak gain of approximately 9 dBi was achieved. Our goal is to design a standing wave antenna with a broadside beam with high gain based on the microstrip lines. Lots of solutions involving the microstrip standing wave array with high gain broadside beams have been reported previously [4]–[7]. However, the feeding networks of these antennas were complex. In this communication, a standing wave linear array integrating the feeding line is introduced. By alternatively blocking the microstrip line every half wavelength, the symmetrical equivalent magnetic currents of the microstrip line are broken for effectively radiating. By properly tuning the blocking positions along the microstrip line, a broadside pattern is achieved with high gain. Compared to the antenna reported in [3] (we call it the reference antenna), the proposed antenna can produce the broadside beam which cannot be achieved with the reference antenna. The reason for this is that the “open stopband” existed in all travelling wave antennas. Moreover, the length of the proposed antenna is halved, but the maximum gain is about 3.5 dB higher.

More importantly, the proposed antenna array has the potential to be built only by metal without any dielectrics. Antennas with all-metal structures have many advantages compared to those made by dielectrics. First, the nonexistence of the dielectric substrates results in fabrication convenience [8]–[15]. Most of the all-metal antennas can be manufactured by the traditional machining process technology such as line cutting, laser cutting and metal stamping, which are all very mature technologies nowadays. Second, antennas without dielectric substrates can achieve excellent performance. In many published communications, all-metal structures with air substrate replace those with dielectric substrates to achieve convenient fabrication, high gain, wide bandwidth, and low dielectric losses [8]–[15]. The merit of low loss is most notable when the operation frequency is high. Wong proposed two very thin internal air substrate mobile phone antennas fabricated by line-cutting a 0.2 mm thick copper plates, resulting in low profiles and wide bandwidths [14], [15]. Third, all-metal antennas have bigger volumes than the counterparts fabricated by using dielectrics, so they have faster heat dissipating performance. In this communication, the proposed antenna is fabricated with all metal. A hand-made model which shows a fraction bandwidth of 11.78% and a maximum gain of 12.47 dBi is built.

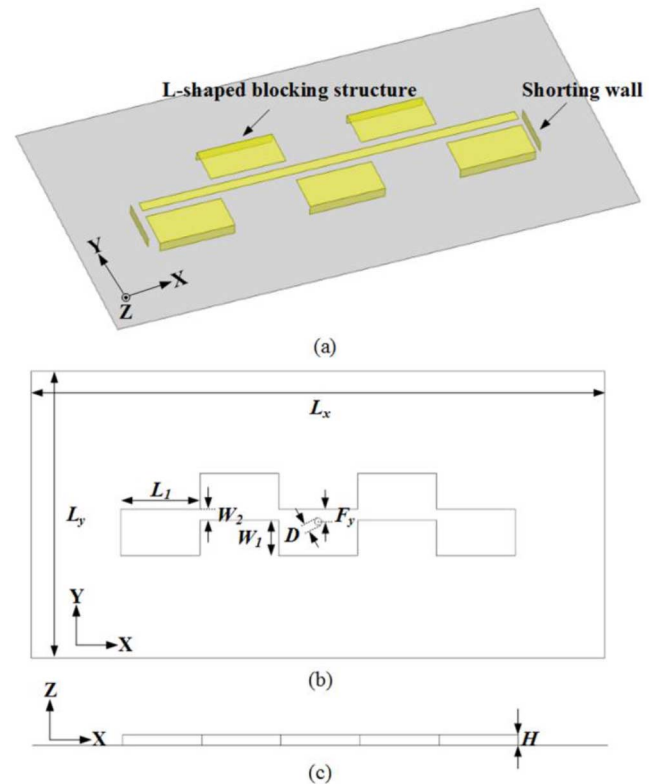


Fig. 2. Geometry of the proposed antenna. (a) Exploded view. (b) Top view. (c) Side view.

TABLE I  
DETAILED DIMENSIONS OF THE PROPOSED ANTENNA

Parameter	$L_x$	$L_y$	$L_1$	$W_1$	$W_2$	$D$	$F_y$	$H$
Value (mm)	160	80	23	11	3	2	3.5	3

## II. ANTENNA DESIGN

Fig. 2(a) shows the exploded view of the proposed antenna, which is composed of a microstrip line, five L-shaped blocking structures, two rectangular shorting walls, and a metallic ground. All constituent parts are separated in order to illustrate the antenna clearly. In fact, all parts are interconnected into a whole. The top and side views are shown in Fig. 2(b) and (c). The width ( $W_2$ ) and height ( $H$ ) of the microstrip line have the same value of 3 mm. The L-shaped blocking structures are used to block the equivalent magnetic currents every half wavelength. In order to obtain in-phase currents, they are arranged alternatively around the microstrip line. Both the head and tail ends are shorted to the ground through two rectangular shorting walls to obtain a good standing wave resonant mode. The L-shaped blocking structures have a length ( $L_1$ ) of 23 mm and a width ( $W_1$ ) of 11 mm, while the rectangular wall has a width ( $W_r = W_1 + W_2$ ) of 14 mm and a height ( $H$ ) of 3 mm. The dimensions ( $L_x \times L_y$ ) of the metallic ground are 160 mm  $\times$  80 mm and the radiating body is centrally aligned with the ground. The hole with a diameter ( $D$ ) of 2 mm is used for feeding. The feeding hole is arranged in the median line of x-direction and 3.5 mm ( $F_y$ ) off from the nearest line edge. A 50- $\Omega$  semirigid cable is used to feed the proposed antenna (Table I).

The simulated magnitude of the reflection coefficient of the proposed antenna from 5 to 9 GHz is shown in Fig. 3. Three resonant points at 5.36, 6.69, and 8.24 GHz are excited. Vector electric field distributions and the corresponding equivalent magnetic currents at

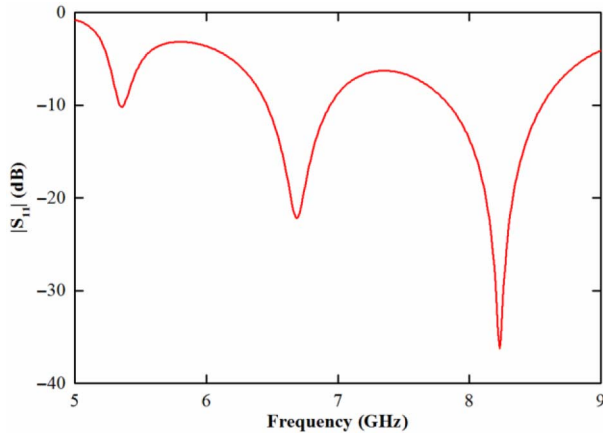


Fig. 3. Simulated magnitude of reflection coefficient of the proposed antenna.

the three frequencies are depicted in Fig. 4(a)–(f), where the equivalent magnetic currents are denoted by black arrow lines and the ground plane is omitted for concision. Fig. 4(a) depicts the vector electric field for the fundamental mode of 5.36 GHz. A half-wavelength standing wave is distributed along the proposed antenna at 5.36 GHz, and the magnetic currents at the five radiating segments are alternatively reversed as shown in Fig. 4(b), resulting in a null in the radiation pattern at the broadside. Fig. 4(c) shows the vector field for the 3-order mode, which operates at the second resonant frequency of 6.69 GHz. Three half-wavelength standing waves are distributed along the proposed antenna. The magnetic currents shown in Fig. 4(d) are alternatively reversed, similar to the situation of the fundamental mode, resulting in a null in the radiation pattern at the broadside as well. The electric field at 8.24 GHz is the 5-order mode, one half-wavelength standing wave is distributed in each segment as shown in Fig. 4(e). Thus, five in-phase magnetic currents are excited as depicted in Fig. 4(f) leading to effective radiation. If the two shorting walls were removed, as can be seen in Fig. 4(g), the electric field at 8.24 GHz is desultory. Six electric nulls occur in the radiating segments, thus, the equivalent magnetic current of each edge is composed of two out-of-phase currents, as illustrated in Fig. 4(h). Therefore, some energy cancel out at the broadside leading to bad performance. Hence, the two shorting walls play a pivotal role.

The operation mechanism is explained as follows. The transmission characteristic of the microstrip line is expected to remain unchanged after bringing in the L-shaped blocking structures, so the ideal width ( $W_1$ ) of the structures is expected to be quarter wavelength, leading to virtual open circuits beside the line. This ideal case refers to that the filed along x-direction is a constant, leading to a zero x-direction wave number ( $k_x = 0$ ). However, the field of a single segment along the x-direction has one half-wavelength standing wave distribution, leading to a positive  $k_x$ . According to the resonator theory,  $k_x^2 + k_y^2 = k_0^2$ . Thus,  $k_y$  is smaller than that of the ideal case, resulting the realistic width ( $W_1$ ) is larger than the ideal value. Here,  $L_1$  is selected freely, and  $W_1$  is adjusted accordingly in order to obtain the virtual open circuit condition and best field distribution.

Some key parameters that have significant effects on the antenna performance are studied. In these parametric studies, only one parameter at a time is varied, whereas the others are kept invariant. The dimensions of the L-shaped structures ( $L_1$  and  $W_1$ ), the width of the microstrip line ( $W_2$ ), and the location of the feeding point ( $Fy$ ) have great influence on the impedance matching, as shown in Fig. 5. As the length and width of the L-shaped structures increase, the resonant frequency decreases, and the optimized length of 23 mm and width of

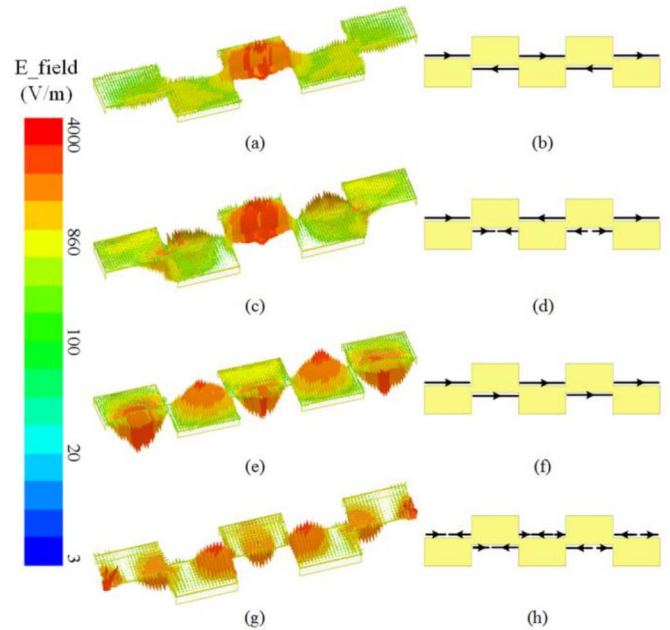


Fig. 4. Vector electric field distributions and their equivalent magnetic currents of the proposed antenna at (a) and (b) 5.36 GHz, (c) and (d) 6.69 GHz, (e) and (f) 8.24 GHz, (g) and (h) 8.24 GHz with the two shorting walls at the end removed. (The equivalent magnetic currents are denoted by black arrow lines, the ground plane is omitted for concision).

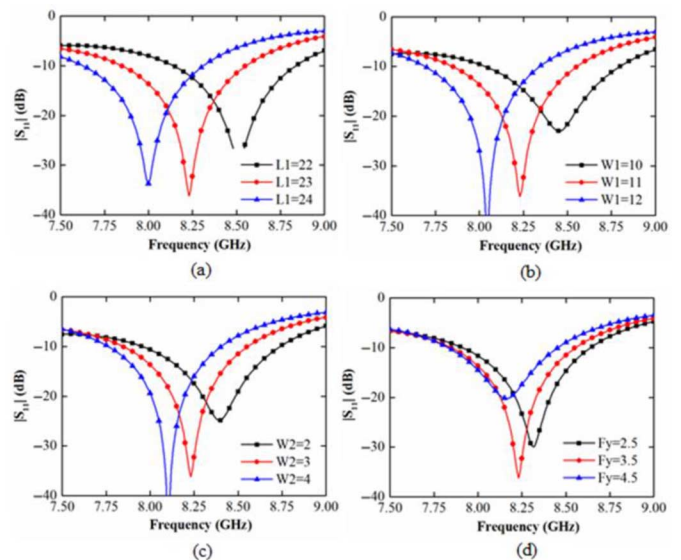


Fig. 5. Magnitude of reflection coefficients with variation of (a)  $L_1$ , (b)  $W_1$ , (c)  $W_2$ , and (d)  $Fy$ . (Unit: mm).

13 mm are selected for the best matching at 8.24 GHz. The change of the microstrip line width alters the characteristic impedance: As the line width changes to 2 or 4 mm, the matching condition gets worse. The location of the feeding point has a great impact on impedance matching. The best location is 3.5 mm away from the edge of the center segment.

The proposed antenna has the advantage of being scalable along the x-direction. Directivities at 8.24 GHz varying with the number of radiating segments (or L-shaped blocking structures) are shown in Table II. The directivity increases as more L-shaped blocking structures are cascaded. The number of radiating segments can be selected according to

TABLE II  
SIMULATED DIRECTIVITY VARYING WITH THE NUMBER OF SEGMENTS

Number	1	3	5	7	9	11	13	15
Directivity (dBi)	8.2	10.3	12.6	13.6	14.3	14.8	15.3	15.5

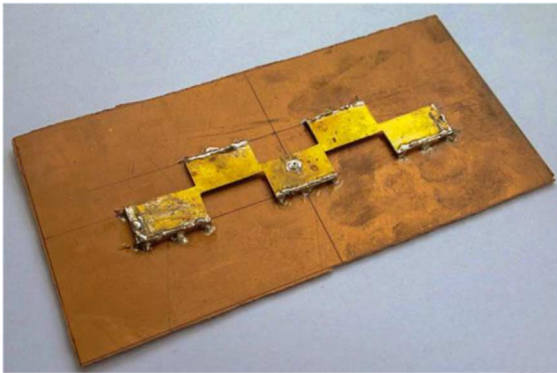


Fig. 6. Prototype of the proposed antenna.

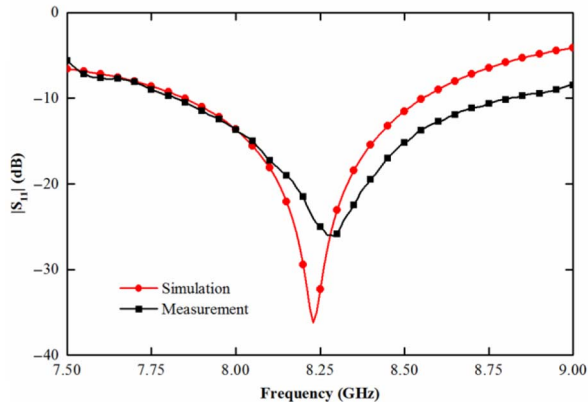


Fig. 7. Measured and simulated magnitude of reflection coefficients.

the desired gain. However, the gain increment is less significant as the segments increase. As the number increases from 13 to 15, the directivity only increases 0.2 dB. This is because the energy coupled to the two ends gets lower as more radiating segments are cascaded. Here, we just make a proof of principle with an example of five segments.

### III. MEASUREMENT RESULTS

A prototype of the proposed antenna shown in Fig. 6 is fabricated manually. The reflection coefficient is measured with an Agilent N5247A vector network analyzer, and the radiation pattern and peak gains are obtained in an anechoic chamber.

Fig. 7 shows the measured reflection coefficient in comparison with the simulated result. The measured and simulated impedance bandwidths are 7.83–8.81 GHz (980 MHz, 11.78%) and 7.84–8.56 GHz (720 MHz, 8.78%), respectively. The measured bandwidth is wider than the simulated one, and the center frequency deviates from 8.24 to 8.39 GHz. The disagreement between the measurement and simulation is caused by fabrication errors. Because the proposed antenna is hand-made, lots of errors may occur, such as the deviation of the feeding location, the uneven top surface, and the imprecise welding between the top surface and the blocking structures. Even so, the measured result is still good enough.

The normalized radiation patterns at 8.24 GHz in the H-plane (XZ) and E-plane (YZ) are presented in Fig. 8. Broadside beams are

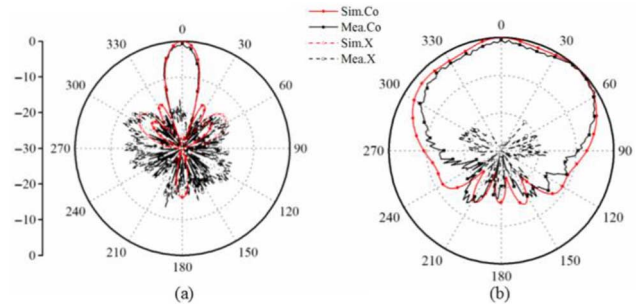


Fig. 8. Measured and simulated normalized co-pol and x-pol radiation patterns of the (a) H-plane, and (b) E-plane.

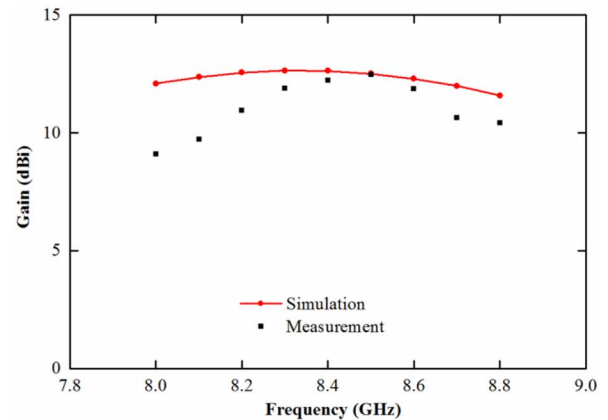


Fig. 9. Measured and simulated peak gains at broadside.

obtained due to the standing wave resonant mode shown in Fig. 4(e). This is one of the main differences distinct from the reference antenna [3]. There is good agreement observed between the measured and simulated results. Fan-shaped beam is observed. The measured and simulated peak gains at 8.24 GHz are 12.47 dBi and 12.62 dBi, respectively. The maximum measured x-pol level is  $-17.78$  and  $-12$  dBi in the E-plane and H-plane, respectively. The x-pol levels are higher than the simulated results owing to the hand-made errors.

Fig. 9 shows the peak gain curve at broadside. The simulated realized gain ranges from 11.59 to 12.62 dBi, and the measured result is a little lower, ranging from 9.1 to 12.47 dBi. The deviation is caused by fabrication and measurement errors.

### IV. CONCLUSION

An all-metal standing wave linear array based on the microstrip lines is proposed. Five L-shaped blocking structures are arranged alternately beside the microstrip line, and the line are shorted to the ground at the head and tail ends. The all-metal structure antenna array has the merits of fabrication convenience, excellent performance, and application suitability where dielectrics are problematic. A broadside pattern with high gain is achieved. The maximum broadside gain of 12.47 dBi is achieved by five radiating segments. The proposed antenna is scalable along one direction to a certain level to acquire the directivity as high as about 15 dBi.

### REFERENCES

- [1] D. M. Pozar, *Microwave Engineering*, 3rd ed. Hoboken, NJ, USA: Wiley, 2005.
- [2] C. A. Balanis, *Antenna Theory*, 3rd ed. Hoboken, NJ, USA: Wiley, 2006.

- [3] Y. X. Li, Q. Xue, E. K.-N. Yung, and Y. L. Long, "The periodic half-width microstrip leaky-wave antenna with a backward to forward scanning capability," *IEEE Trans. Antennas Propag.*, vol. 58, no. 3, pp. 963–966, Mar. 2010.
- [4] H. Legay and L. Shafai, "Planar resonant series-fed arrays," *Proc. Inst. Electr. Eng.*, vol. 144, no. 2, pp. 67–72, Apr. 1997.
- [5] K. Wincza and S. Gruszczynski, "Microstrip antenna arrays fed by a series-parallel slot-coupled feeding network," *IEEE Antennas Wireless Propag. Lett.*, vol. 10, pp. 991–994, Oct. 2011.
- [6] I. Slomian, K. Wincza, and S. Gruszczynski, "Series-fed microstrip antenna array with inclined-slot couplers as three-way power dividers," *IEEE Antennas Wireless Propag. Lett.*, vol. 12, pp. 62–64, Mar. 2013.
- [7] I. Slomian, K. Wincza, and S. Gruszczynski, "Series-fed microstrip antenna lattice with switched polarization utilizing Butler matrix," *IEEE Trans. Antennas Propag.*, vol. 62, no. 1, pp. 145–152, Jan. 2014.
- [8] M. S. R. Palacios and M. J. M. Silva, "Air substrate patch and monopole antennas in compact array for MIMO applications," in *Proc. IEEE Elect. Eng. Comput. Sci. Autom. Control (CCE)*, Tuxtla, Gutierrez, Sep. 2010, pp. 305–308.
- [9] S. Y. Lin and K. L. Wong, "Effects of slotted and photonic bandgap ground planes on the characteristics of an air-substrate annular-ring patch antenna at TM<sub>21</sub> mode," in *Proc. IEEE Asia-Pac. Microw. Conf.*, Taipei, Taiwan, Dec. 2001, vol. 2, pp. 655–658.
- [10] F. W. Yao, S. S. Zhong, and X. L. Liang, "Ultra-broadband patch antenna using a wedge-shaped air substrate," in *Proc. IEEE Asia-Pac. Microw. Conf.*, Dec. 2005, pp. 1–3.
- [11] K. Nishizawa, H. Ohashi, and Y. Konishi, "An orthogonal dual polarized all-metal cavity-backed patch antenna with low cross polarization," in *Proc. IEEE Antennas Propag. Soc. Int. Symp. (APSURSI)*, San Diego, CA, Jul. 2008, pp. 1–4.
- [12] D. Guha, S. Chattopadhyay, and J. Y. Siddiqui, "Estimation of gain enhancement replacing PTFE by air substrate in a microstrip patch antenna [antenna designer's notebook]," *IEEE Antennas Propag. Mag.*, vol. 52, no. 3, pp. 92–95, Jun. 2010.
- [13] C. Chandan, A. Ghosh, S. K. Ghosh, and S. Chattopadhyay, "Radiation characteristics of rectangular patch antenna using air substrates," in *Proc. IEEE Int. Conf. Emerg. Trends Electron. Photon. Devices Syst.*, Varanasi, Dec. 2009, pp. 346–348.
- [14] K. L. Wong, Y. C. Lin, and T. C. Tseng, "Thin internal GSM/DCS patch antenna for a portable mobile terminal," *IEEE Trans. Antennas Propag.*, vol. 54, no. 1, pp. 238–242, Jan. 2006.
- [15] K. L. Wong, Y. C. Lin, and B. Chen, "Internal patch antenna with a thin air-layer substrate for GSM/DCS operation in a PDA phone," *IEEE Trans. Antennas Propag.*, vol. 55, no. 4, pp. 1165–1172, Apr. 2007.

## Single-Feed Ultra-Wideband Circularly Polarized Antenna With Enhanced Front-to-Back Ratio

Long Zhang, Steven Gao, Qi Luo, Paul R. Young, Qingxia Li, You-Lin Geng, and Raed A. Abd-Alhameed

**Abstract**—This communication presents a single-feed ultra-wideband circularly polarized (CP) antenna with high front-to-back ratio (FBR). The antenna is composed of two orthogonally placed elliptical dipoles printed on both sides of a substrate. To realize high FBR, a novel composite cavity is also proposed and integrated with the presented crossed dipoles, which effectively reduces the backlobe of the crossed dipoles. Simulation results are in good agreement with the measured results that demonstrate an impedance bandwidth from 0.9 to 2.95 GHz (106.5%) and a 3-dB axial ratio (AR) bandwidth from 1 to 2.87 GHz (96.6%). The measured FBR is about 30 dB across the whole global navigation satellite system (GNSS) band. Compared with other reported single-feed wideband CP antennas, the antenna has advantages such as a wider CP bandwidth and lower backlobe radiation.

**Index Terms**—Backlobe reduction, circular polarization, crossed dipoles, single-feed antennas, wideband antenna.

### I. INTRODUCTION

Circularly polarized (CP) antennas are widely used in global navigation satellite systems (GNSSs), RFID, satellite communication systems, and wireless power transmission systems due to their capabilities of reducing polarization mismatch and suppressing multipath interferences [1].

Generally, the CP antennas can be divided into two categories: single feed and multifeed. With the trend of increasing capacity of various wireless communication systems, the bandwidth of CP antennas needs to be enhanced. However, it is always challenging to design a broadband CP antenna with single feed. One type of single-feed broadband CP antenna is the spiral antenna. However, their bidirectional radiation properties make these conventional spiral antennas unsuitable for some applications such as GNSS application since a directional radiation pattern is needed to decrease the effects of the reflections from the ground [2]. Several directional spiral antennas including spiral-mode microstrip (SMM) antenna [3], conducting plane backed spiral [4], and cavity backed spiral [5] have been proposed to conquer this problem. Another issue of the spiral antennas is the need for a balun that increases the complexity of the spirals.

Recently, a single-feed crossed dipole with integrated phase delay line was presented in [6]. This antenna can achieve more than 15% 3-dB axial ratio (AR) bandwidth with a simple feeding structure. To enhance the bandwidth, parasitic loops are introduced and a 28.6%

Manuscript received March 13, 2015; revised September 28, 2015; accepted November 11, 2015. Date of publication November 19, 2015; date of current version December 31, 2015.

L. Zhang, S. Gao, Q. Luo, and P. R. Young are with the School of Engineering and Digital Arts, University of Kent, Canterbury CT2 7NT, U.K. (e-mail: lz76@kent.ac.uk; s.gao@kent.ac.uk; qiluo@ieee.org; p.r.young@kent.ac.uk).

Q. Li is with the School of Electronic Information and Communications, Huazhong University of Science and Technology, Wuhan 430074, China.

Y.-L. Geng is with the Institute of Antenna and Microwaves, Hangzhou Dianzi University, Hangzhou 310018, China.

R. A. Abd-Alhameed is with the University of Bradford, Bradford BD7 1DP, U.K.

Color versions of one or more of the figures in this communication are available online at <http://ieeexplore.ieee.org>.

Digital Object Identifier 10.1109/TAP.2015.2501844